Supporting Information

Current Detection Technologies of Circulating Tumor Cells

Zheyu Shen,[a,b] Aiguo Wu,[a,*] Xiaoyuan Chen[b,*]

[a] CAS Key Laboratory of Magnetic Materials and Devices, & Key Laboratory of Additive Manufacturing Materials of Zhejiang Province, & Division of Functional Materials and Nanodevices, Ningbo Institute of Materials Technology and Engineering, Chinese Academy of Sciences, 1219 ZhongGuan West Road, Ningbo, Zhejiang 315201, China.

[b] Laboratory of Molecular Imaging and Nanomedicine, National Institute of Biomedical Imaging and Bioengineering, National Institutes of Health, Bethesda, Maryland 20892, United States.

Corresponding Authors

*E-mail: shawn.chen@nih.gov.

*E-mail: aiguo@nimte.ac.cn.

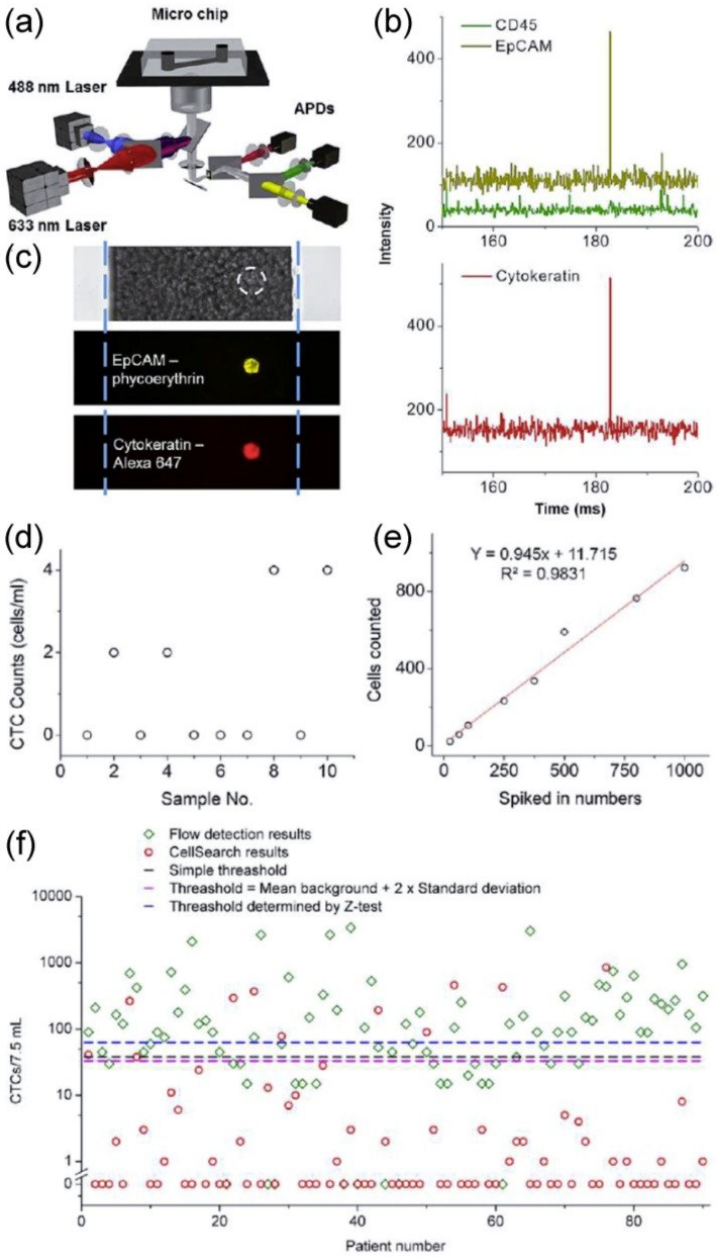

Figure S1. Schematic and data illustrating the CTC direct detection technology by line-confocal microscope. (a): Illustration of the devices including the microfluidics and optics. (b): Avalanche photodiodes (APD) signals for CTC detection. (c): Cell imaging of the MCF-7 cell in whole blood that was filled in the microfluidic channel. (d): False positive of the CTC counting. (e): Recovery performance of the CTC counting (i.e. the counted CTC numbers VS the spiked CTC numbers). (f): Clinical results of the CTC analysis on 90 blood samples from 24 breast cancer patients by the line-confocal microscope (i.e. flow counting system) or CellSearch system. Reproduced from reference 23 with permission from American Chemical Society, copyright 2013.

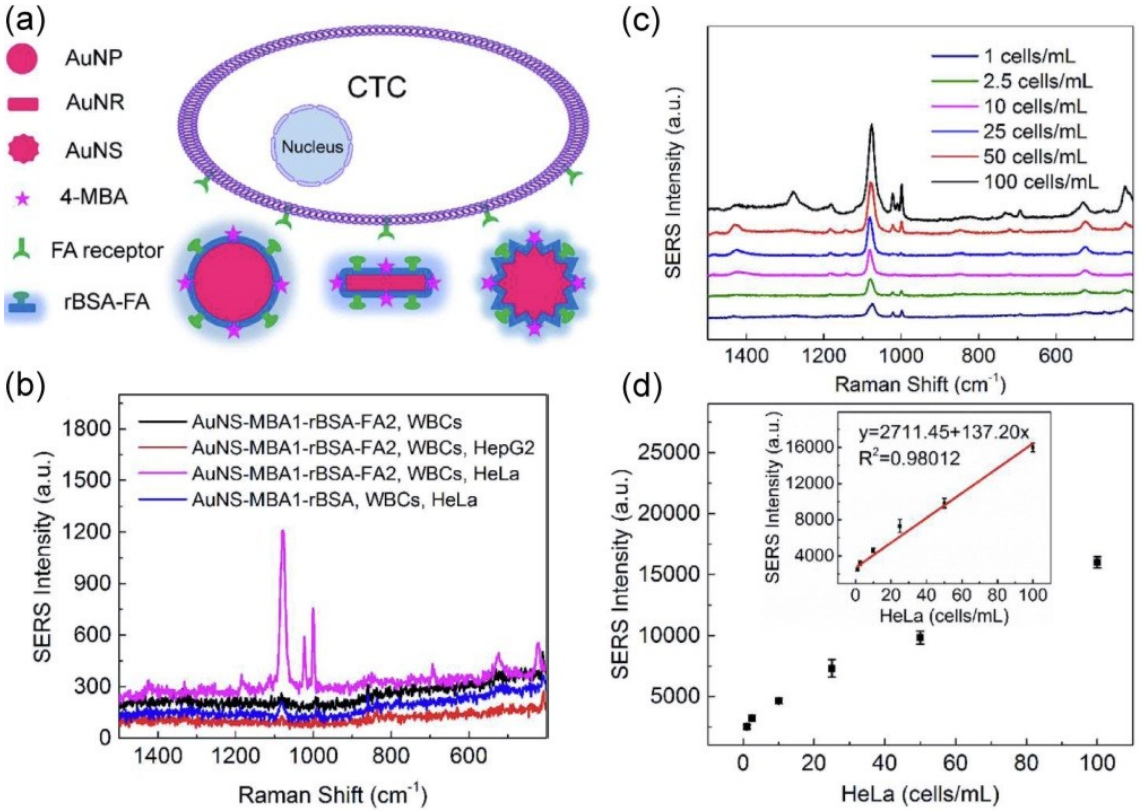

Figure S2. Design of the SERS nanoparticles with various shapes (a), and specificity (b) and sensitivity (c, d) of the SERS-active AuNSs for CTC direct detection in blood samples. (b): SERS signals of the AuNS-MBA1-rBSA nanoparticles with or without conjugation of targeting ligand FA in rabbit blood samples (4.0 mL) with or without spiking of 4 HeLa cells (or 4 HepG2 cells); (c): SERS signals of the AuNS-MBA1-rBSA-FA2 nanoparticles in the rabbit blood (4.0 mL) with spiking of 1-100 HeLa cells/mL; (d): Plot of the intensity of SERS signals as a function of the HeLa cell concentration spiked into the rabbit blood. Reproduced from reference 27 with permission from American Chemical Society, copyright 2016.

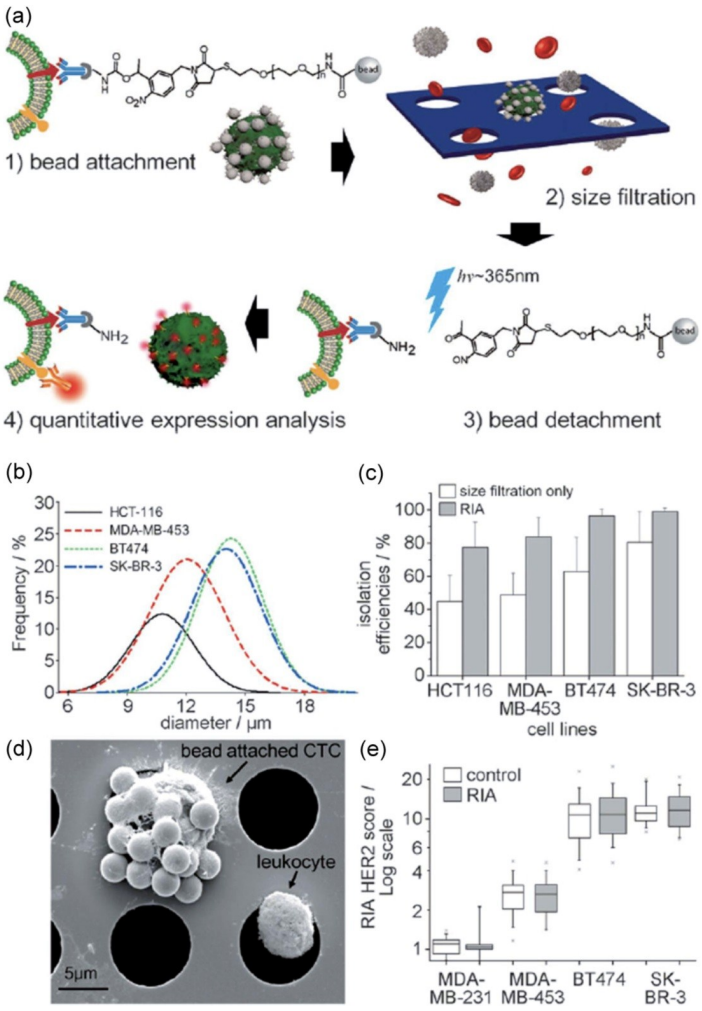

Figure S3. (a): Illustration of CTC isolation and subsequent in situ protein expression analysis using RIA. 1) Detachable beads bind to CTCs by conjugated antibodies; 2) Bead-attached cells are filtered through a membrane filter chip; 3) Exposure to i-line irradiation induces photo cleavage of the linker between the bead surface and the conjugated antibody, resulting in bead detachment from CTCs; 4) Isolated CTCs are immunostained and their in situ protein-expression levels are assessed. (b): Distribution of cell diameters for four different cell types. (c) Comparison of isolation efficiencies between conventional size-based exclusion and RIA. (d) SEM image of a CTC isolated by the RIA platform. (d) Comparison of fluorescence signal intensities in control and RIA-processed cells for cancer cells with different levels of HER2 expression. Reproduced from reference 1 (in Supporting Information) with permission from Wiley-VCH Verlag GmbH & Co. KGaA, Weinheim, copyright 2013.

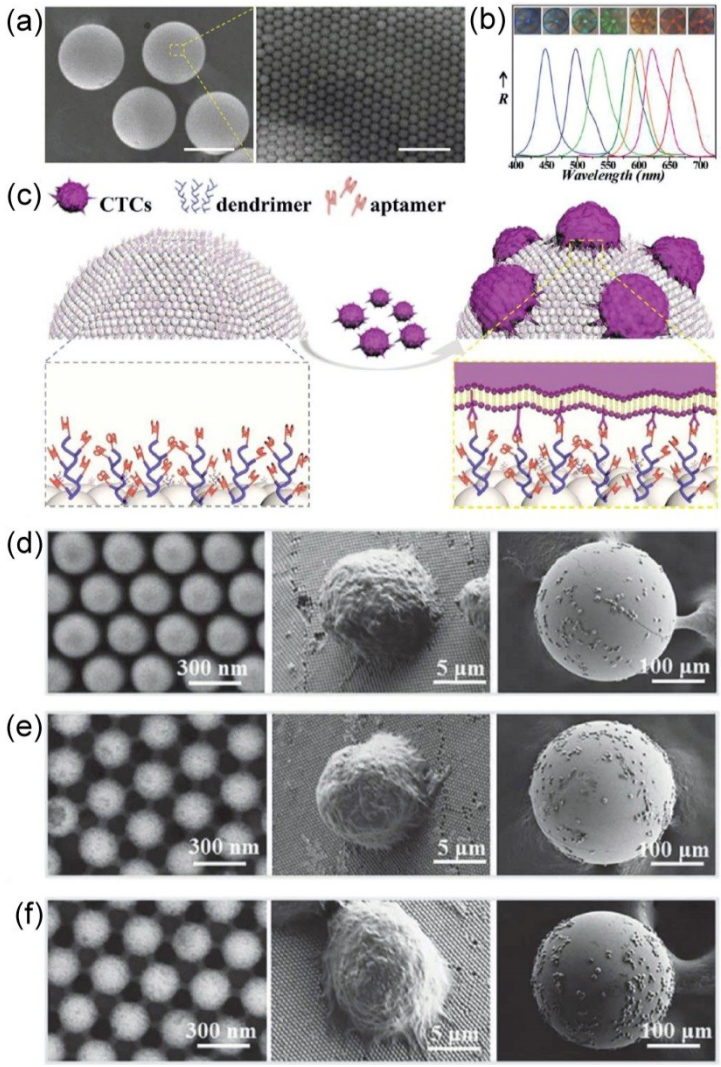

Figure S4. (a): Scanning electron microscopy (SEM) images of the barcode particles (left) and of the enlarged nanostructure surface of the barcode particles, revealing the nanoparticle array (right). Scale bars are 200 μm (left figure) and 1 μm (right figure). (b): Microscopy images (insets) and reflection spectra of seven different types of barcode particles. (c): Schematic of the barcode particles used for enhanced CTC capture; the surface of the barcode particles is decorated with dendrimer and DNA aptamers. (d-f): Field-emission SEM (FESEM) images of the surface nanostructure (left row), of the morphology of a captured CTC (middle row), and of the distribution of the CTCs (right row) of various barcode-particle substrates. (d): untreated barcode particles decorated with aptamers. (e) etched barcode particles decorated with aptamers. (f) etched barcode particles decorated with dendrimers and aptamers. Reproduced from reference 43 with permission from Wiley-VCH Verlag GmbH & Co. KGaA, Weinheim, copyright 2014.

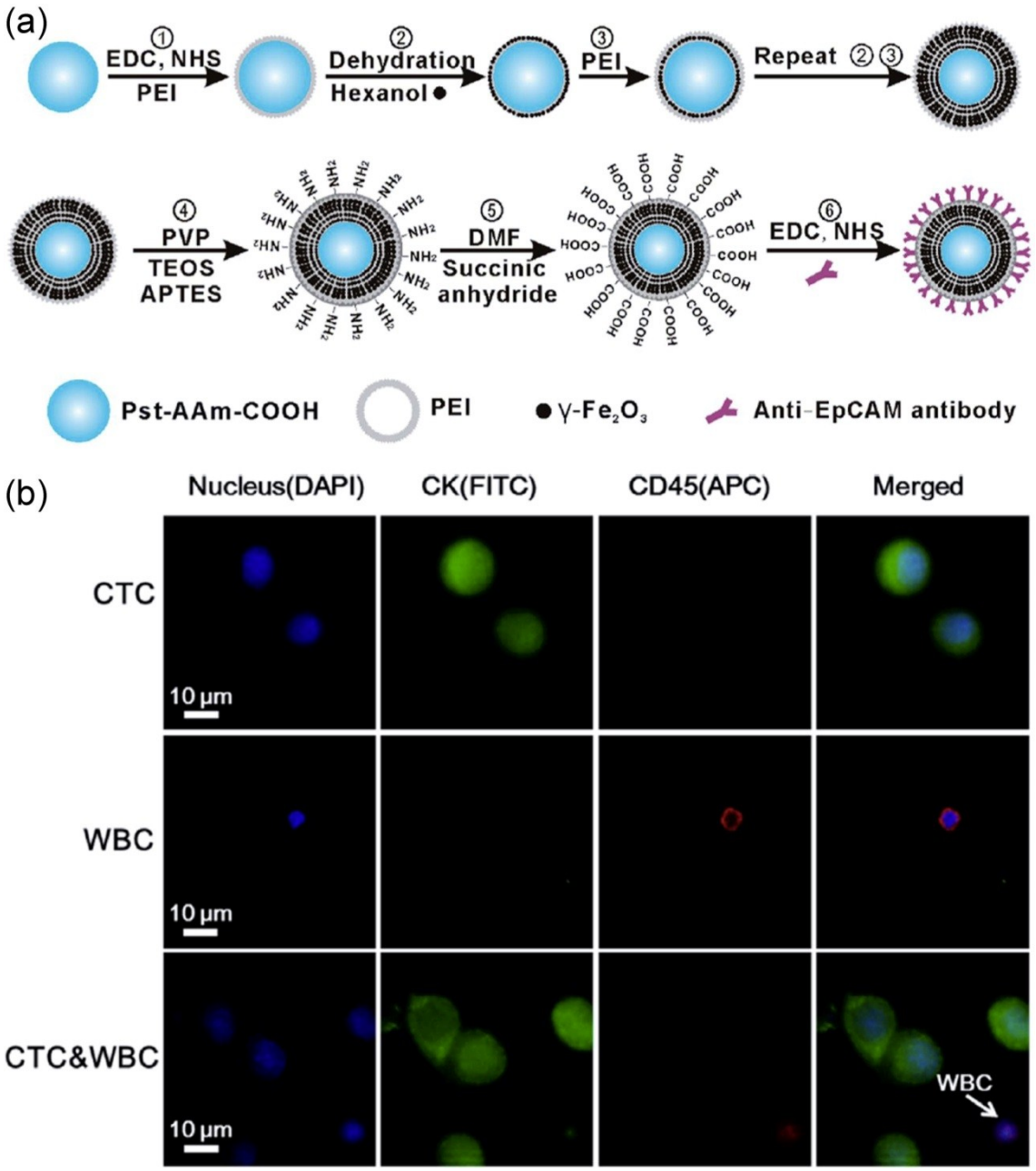

Figure S5. (a): Schematic diagram for the construction of immunomagnetic nanospheres. (b): Confocal microscopic images of cells captured from mimic clinical blood samples and identified with the three-color ICC. Nucleus (DAPI): excitation 405 nm, emission 447±30 nm band-pass. CK (FITC): excitation 488 nm, emission 525±25 nm band-pass. CD45 (APC): excitation 605 nm, emission 685±20 nm band-pass. Merged: merge of nucleus (DAPI), CK (FITC), and CD45 (APC). Reproduced from reference 2 (in Supporting Information) with permission from American Chemical Society, copyright 2013.

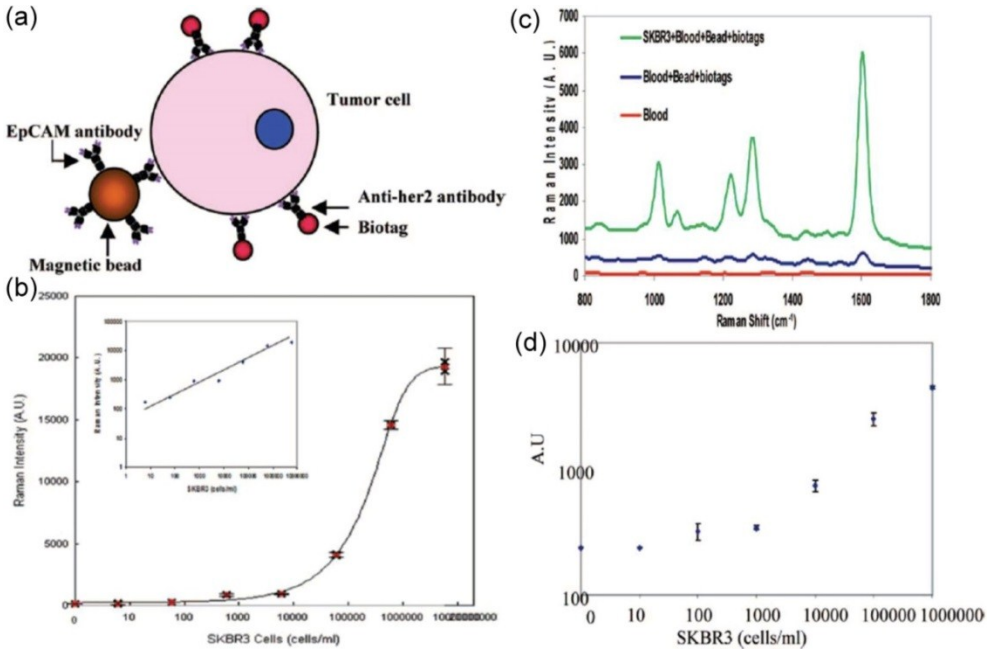

Figure S6. (a): Schematic illustration of the ternary immuno-complex formed by nanoplex biotags and magnetic bead conjugates binding to the model tumor cell. (b): Detection of CTCs in buffer. Dose-response curve of SKBR3 cells spiked into buffer. (c): Detection of SKBR3 spiked into whole blood. Raman spectra of whole blood (red) and of beads and biotag reagents in blood without a cell spike (blue) and with SKBR3 cells spike (green). (d): Dose-response curve of SKBR3 cells spiked into whole blood. Blood with no cell spike was used as a negative control. Reproduced from reference 20 with permission from American Chemical Society, copyright 2008.

References

[1] H. J. Lee, J. H. Oh, J. M. Oh, J. M. Park, J. G. Lee, M. S. Kim, Y. J. Kim, H. J. Kang, J. Jeong, S. I. Kim, S. S. Lee, J. W. Choi and N. Huh, Efficient isolation and accurate in situ analysis of circulating tumor cells using detachable beads and a high-pore-density filter, *Angew. Chem. Int. Ed.*, 2013, **52**, 8337-8340.

[2] C. Y. Wen, L. L. Wu, Z. L. Zhang, Y. L. Liu, S. Z. Wei, J. Hu, M. Tang, E. Z. Sun, Y. P. Gong, J. Yu and D. W. Pang, Quick-response magnetic nanospheres for rapid, efficient capture and sensitive detection of circulating tumor cells, *ACS Nano*, 2014, **8**, 941-949.